JOURNAL OF SPACECRAFT AND ROCKETS
Vol. 44, No. 4, July–August 2007

Validation of a Scalable Solar Sailcraft System

David M. Murphy*
ATK Space Systems and Sensors, Goleta, California 93117

DOI: 10.2514/1.23024

To enable certain near- and midterm NASA space science missions by significantly reducing cost, mass, and travel times, NASA's In-Space Propulsion Technology Program sponsored intensive solar sail systems technology design, development, and hardware demonstration activities over a period of three years. For the first time, the rigorous validation of a scalable three-axis stabilized solar sail system, through functional evaluations in relevant environments together with analysis correlation activities, was achieved. This paper presents a review of the design developed, results of testing, and analytical validations of component and assembly functional, strength, stiffness, shape, and dynamic behavior. The scaled performance of the validated system is projected to demonstrate readiness for flight demonstration and applicability to NASA road-map missions.

I. Introduction

AT THE start of 2003, ABLE Engineering (now part of ATK Space Systems and Sensors), in parallel with other activities [1] also under the purview of the In-Space Propulsion (ISP) projects office at NASA Marshall Space Flight Center (MSFC), began developing scalable analytical tools and advanced design technologies for a solar sail system, which led to two follow-on phases for system ground demonstrator (SGD) development and validation. These efforts, led by ATK, were performed with the assistance of the Systems Technology Group of SRS Technologies (the sail assembly provider), the NASA Langley Research Center (LARC) for sail shape and dynamics modeling and test execution, Arizona State University (ASU) for attitude-control modeling, Princeton Satellite Systems (PSS) for sailcraft control software, and the NASA Marshall Space Flight Center (MSFC) space environmental effects (SEE) laboratory (materials characterization and life evaluation).

In the first phase of the program (six months), activities were focused on design and analysis refinement of the initial sail system concept [2] and refinement of plans for hardware development and demonstration [3] in phases 2 and 3. The phase 2 effort encompassed design, fabrication, and validation *through a series of component and system tests* of a quadrant (one sail and two masts) of a 10-m system. Validation activities culminated with the demonstration of deployment, sail shape, and system dynamics measurement [4] in a vacuum at the LARC in April of 2004 [5]. Analytical correlation activities demonstrated that gossamer mast, sail subassemblies, and system behavior are predictable [6].

In phase 3, a larger and more complete sail system was designed, fabricated, and demonstrated [7], first in ambient conditions at ATK in Goleta, CA (ATK-Goleta) and later at a large vacuum-chamber facility in April and May of 2005. The 20-m sailcraft hardware represents a flightworthy full (four sails, four masts) system that includes a boom for offsetting instruments well away from the plane of the sail, a dual-purposed mechanism for deployment and attitude control, tie-down and release hardware, solar panels, and launch vehicle interfaces, which were integrated in a carbon-composite central assembly that also functions as a bus chassis.

Further descriptions of the hardware are provided herein, along with a review of some of the critical design developments important to the evolution and success of the SGD efforts. Lessons learned in the development of subsystem hardware on a quadrant of a 10-m sail system, referred to herein as the 10-m quadrant, were integrated into design and analysis activities supporting the fabrication and testing of the full sail system. The evolution and integration of additional subsystems included in the 20-m sailcraft are described. Results of 20-m sailcraft system validation activities are emphasized, followed by sail-material life-testing results, discussion of scaled performance, and concluding remarks.

II. Technology Maturation

The ISP projects office at NASA headquarters prioritized the maturation of solar sail propulsion technology readiness to enable or enhance a variety of road-mapped space science missions [8,9]. Solar sails, especially as a system, present complex engineering challenges. In particular, the difficulty of validating finite element analysis (FEA) modeling *through testing in a fully representative environment before flight* has thus far discouraged near-term mission planners from using this enabling propulsion technology.

The ground system demonstration and validation accomplishments of the S^4 SGD program were planned to systematically reduce the risk of flight implementation through building increasingly more complex solar sail systems together with testing of the highest fidelity possible in the terrestrial environment. The progression of major hardware builds over the program is depicted in Fig. 1. Incremental design and demonstration were pursued to minimize cost and risk while methodically elevating the technology readiness level (TRL) of dependent systems before full-system demonstration.

Early in the first hardware development cycle (phase 2 of the three-phase program), CP1† sails and prototype carbon-fiber coilables (truss structures named for their form during intermediate states of deployment) were assembled and tested. Phase 2 culminated in the building and testing of a quarter-symmetry deployable system 10 m from mast tip to mast tip. The quarter-symmetry of the S^4 system allowed a quadrant to be built that validated fundamental aspects of the full system while minimizing overall costs. In the third phase, a complete 20-m S^4 system was built and rigorously tested, validating both the hardware design and the scaled analytical and computer models. Testing activities in phase 3 included sail-assembly deployment trials at SRS and subsystem evaluations at ATK. The activities were conducted before and during system integration and checkout, launch venting was at Wyle Laboratory, and vibration testing was at Environmental Associates. Moreover, and most important, these activities were conducted before and during system deployment, functional demonstrations, and shape and dynamics

Received 7 February 2006; revision received 2 September 2006; accepted for publication 12 October 2006.

*Chief Research Engineer, 600 Pine Avenue; dave.murphy@atk.com. Member AIAA.

†CP1 is a colorless polyimide material developed by the NASA LARC to meet requirements for a transparent material that exhibits improved thermal stability and greater resistance to radiation and atomic oxygen in orbit.

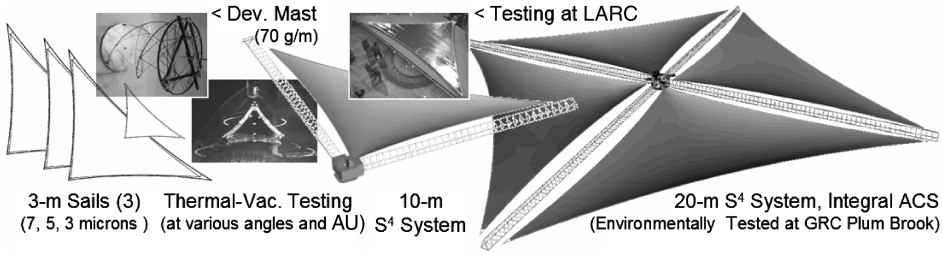

Fig. 1 ISP program milestones: progressive growth in technology maturation, size, and complexity.

measurements in the 100-ft-diam thermal-vacuum chamber at the NASA John H. Glenn Research Center's (GRC) Plum Brook facility. Extensive membrane evaluations and life testing [10] at the SEE laboratory took place in parallel with phases 2 and 3, the results of which are summarized herein.

III. Subsystem Development and Demonstration

As mentioned earlier, S^4 hardware subsystems were designed and demonstrated incrementally in the three-phase ISP program. After the studies were completed in the six-month phase-1 period, key subsystem technologies were built and demonstrated in phase 2: two engineering development unit (EDU) masts and a number of sail assemblies. Next, longer masts and a thinner, refined sail assembly were built and integrated into a deployable quadrant of the symmetric sail system, as shown in Fig. 1. The central assembly was a rudimentary structure of aluminum plates, which served as housing for the stowed masts and sail, and the mechanism necessary for their deployment. It was left to the third phase of the program to develop a flight-representative carbon-fiber-composite central structure, and to add other mechanisms (e.g., ACS actuators). These advancements, together with larger, lighter sails and longer masts, allowed the S^4 sailcraft systems to be completely demonstrated.

The 10-m sailcraft system consisted of three major subassemblies: the sail assembly, two mast assemblies, and the central assembly. The 7-m carbon-fiber-composite mast was (as for the 20-m system) a truncated length of structure, optimized for an 80-m sail system. The sail was composed of an aluminized 3-μm CP1 membrane with integral shear-compliant borders and carbon-fiber edge cords. The subassemblies and the system were put through a complete series of ambient and vacuum testing. The design features and evolution of the mast and sail hardware are discussed next, followed by the results of subsystem and 10-m quadrant testing.

A. Mast

The sail masts are an advanced version of the continuous coilable longeron structures that have flown 27 times in space, with 100% success. The primary change is the substitution of carbon-fiber pultrusion for the heritage S2-glass-fiber structural elements (longerons and battens). The *carbon-fiber* coilable design is the minimum-mass structural configuration appropriate for the gossamer-type loading of a typical sail mission. The coilable mast is a very mass-efficient elemental structure: a 34 g/m sail mast with bending stiffness greater than $10,000\ \mathrm{N \cdot m}$ has been demonstrated [11]. This mass is less than one-seventh of the mass of an equivalent-diameter heritage design (S2-glass-fiber) coilable.

EDUs of the new mast were developed and tested first, before the units for the quadrant were fabricated. The first ultralight carbon-fiber coilable was constructed of an off-the-shelf composite material, because the focus was on new ultralight concepts for the structural joints along the longeron at the interface of the battens and diagonals. This "node" design, which was also radically optimized for mass production, proved unsatisfactory in strength and kinematic reliability. A second EDU, also 10 bays in length, was built with fittings derived from flight-heritage masts, but sized much smaller and composed of magnesium alloy. The function and strength of these new lightweight fittings (less than 10% of the mast mass) proved robust. This mast also successfully demonstrated new structural members (longerons and battens) made of custom-pultruded Hexcel IM9 carbon-fiber-epoxy composite. The linear mass of this 40-cm-diam mast design was 70 g/m. The functional validation of this new gossamer sail-mast design provided the confidence needed to proceed with the fabrication of the two 7-m, 31-bay masts needed for the 10-m quadrant assembly. This mast design was carried forward for the 20-m sailcraft system as well. Therefore, the results of EDU and 7-m mast testing, reviewed in detail in [4], are directly applicable to the phase-3 14-m masts. The 7-m masts met the expected linear compaction factor (0.85%) when stowed. Deployments were performed horizontally, with an overhead rail car for tip offloading. The masts, which self-deploy due to strain energy stored when coiled, were found by measurement to provide a push force of nominally 7 lb, as was predicted by closed-form calculations. Stiffness and strength were evaluated using lateral tip deflections imparted by a simple setup consisting of a pulley and various weights. The deflections were measured using a laser tracking system that followed a retroreflector mounted on the mast-tip ground-support equipment (GSE). Because the 7-m masts are self-supporting in 1 g, free vibration could also be documented with the laser tracker. The frequency of the first bending mode was measured. The bending stiffness EI could not be measured directly by using a lateral tip loading, because one-third of the compliance at this length is due to mast shear stiffness GA. A pretest FEA model of the mast, which captured shear and bending compliance, was used to predict the dynamic behavior. Test data reduction revealed close agreement between the measured and predicted first mode, demonstrating that the coilable performance is a very predictable, readily modeled, linearly behaving structure. It should be noted that longer masts and/or substantially lighter designs are susceptible to stiffness, *and hence also strength*, reduction due to local and global imperfections [12]; a subject under extensive investigation through NASA's New Millennium ST8 program. A key feature of the coilable is that the *open lattice* eliminates the possibility of asymmetric thermal loading, in which sun-side vs shade-side thermal strains induce bow. A potential for thermal-strain-induced bow arises if the sun position is such that one structural element shades another. This problem can be overcome by building a 180-deg twist into the overall length of the mast, an approach that has flown successfully several times.

B. Sail

In efforts parallel with the EDU masts, SRS Technologies began developing fabrication equipment and processes for the assembly of the sails. The first ISP program sail incorporated a 5-μm-thick sail material, adhesiveless seaming processes, and new border and cord designs. This sail assembly, named the Workhorse Sail, was critical for the timely development of packaging and deployment methods. Various further developments in design and fabrication methods were incorporated on a second 5-μm-thick sail. In particular, sequencing elements developed using the Workhorse (to provide a managed deployment) were incorporated. This refined sail (RS5) and a third sail (denoted by RS3) incorporating 3-μm film and further upgrades were both used for system-level test and modeling correlation performed at the LARC.

The CP1 sail material, produced under exclusive license from NASA by SRS Technologies, has had significant space-environment exposure in both real and simulated environments. More than $10,000\ \mathrm{ft^2}$ of material (less than 3-mil thick) has flown on Boeing GEO spacecraft since 1999. The material has been flight-qualified for a 15-year exposure in a GEO environment. In addition, the NASA

ISP program has done extensive testing of sail-gauge (less than 3 μm) CP1 material in simulated ultraviolet (UV) and radiation environments [10].

The sails built were all configured as triangular "quadrants" with scalloped edges and a structural attachment at each corner. A strong motivation behind the selection of a three-point-attachment configuration is to ensure planarity, regardless of intrasail optical or mechanical anisotropy, system orientation to the sun, and thermal cycling. The border scallops are trimmed with high-strength carbon-fiber cords that impart robustness for handling and deployment. Inboard of the cords is a corrugated border area that facilitates decoupling of thermal and mechanical strain between the cord and the main sail [13]. These features provide a nearly uniform stress distribution in the sail, ensuring predicable shape and high propulsive efficiency. When designed with a modest scallop (90% sail-area fill factor), the border imparts these beneficial conditions without significantly increased boom loads. Sequencers (located along the borders in the final design) control the deployment of the sail. The sequencers are staged deterministically so that the delicate sail material is kept away well from the masts. Deployment, stowage (in a matter of hours), and redeployment are robust, reliable, and repeatable.

The sails are electrically grounded via the halyards to the mast and the tack line to the drum, which are part of the structural path linked to the spacecraft ground. Grounding of the joined membrane sections is achieved through the combination of conductive adhesive patches between materials that bridge the conductive aluminum coating and mechanical grommet connections that attach to the three halyard corner attachment points. This method was verified on multiple sails made for the ISP program, for which only the coated side of the membrane was grounded. The antisun side of the sail was left uncoated to maximize thermal emission from the base CP1, which is optically clear. The necessity of rear-side, or bulk, sail conductivity has been debated by leading electrostatics engineers. SRS has developed methods for enhancing the bulk conductivity of CP1 by the addition of carbon nanotubes to the resin matrix. This process provides a surface resistivity in the range of 10^6 Ω (per square), which can be used to reduce risks from plasma interactions. In addition, this black CP1 has a greatly increased emissivity, which allows closer solar-approach mission trajectories.

A solar sail quadrant is necessarily constructed of an extremely thin and therefore delicate membrane. The fundamental challenges are to fold for compact stowage and launch survivability, *ideally, with a process that is time- and manpower-efficient, as well as scalable*, and to construct a convincing ground-test program given the significant effects of gravity on membrane stress and shape and the resistance to movement of the film imposed by the atmospheric density. When deploying on-orbit, the kinematics must insure low mast loading with reliable and deterministic staging throughout the deployment sequence. Most critically, the approach must support the key metric for a solar sail: low areal mass density. The ATK–SRS team developed and tested a number of different approaches over the course of the program, which finally supported all of the goals necessary for robust high-performance sail systems. The evolution in the stowage and deployment design and functionality from the Workhorse Sail to the final 20-m sail is detailed in [3,5,7,13,14]. The specific placement and design of the sequencers used on the 20-m sail is depicted in Fig. 5 of [7]. The solar sail quadrant is folded for stowage first in lines that run parallel to the midline (bisector). Such folding can also apply to the manufacture of the sail, which means the assembly room need only be about half as long as the characteristic sailcraft dimension (mast tip to tip) and as wide as two sections of membranes being joined. The folded sail is rolled onto a lightweight carbon-composite cylindrical "drum," which is installed into the central structure. The stowage procedure is time- and manpower-efficient and completely scalable to ever-larger sail sizes. Sequencing elements are distributed on the perimeter of the sail, for which the strength is substantial due to the embedded cord. This placement allows the main sail to be constructed of the thinnest producible materials to obtain the lowest areal mass density. When deploying the sails on-orbit, the low-force sequencer releases will insure low mast loading with reliable and deterministic staging throughout the deployment sequence.

IV. Demonstration and Validation of 10-Meter Quadrant

After completion of the mast and sail subassembly validations in phase 2, the integrated 10-m quadrant was prepared for testing. To validate deployment characteristics, as well as sail shape and system dynamics, a series of tests was planned using a vacuum chamber facility at the LARC. Testing in a vacuum is necessary because the dynamics of the deploying and deployed sails would otherwise be greatly affected by the surrounding air mass. The air within 2 mm of either side of the sail surface is alone equal in mass to a 3-μm sail film. All sail-dynamics testing at the LARC took place at pressures near 1 torr. The priorities for testing were to first, validate the deployment; second, measure the deployed shape of the (horizontal) sail billowed under gravity loading; and third, validate the models used to predict the system dynamics.

The ABLE-LARC test team planned an extensive series of tests to capture the data needed to support these priorities, as well as to meet goals for developing test methods applicable to 20-m-sail testing and to in-flight investigations.

The testing sequence and findings are reported in detail in [4,5]. In summary, formal testing at the LARC on the 10-m quadrant began on 30 March 2004 with an ambient deployment of the system to verify the GSE setup after shipment and installation in the vacuum chamber. During deployment, a large tear was caused by a sequencer that failed to release, which led to a sequencer redesign. The improved design is discussed in [7].

With the system deployed in a horizontal configuration, measurement of the shape of the surface was undertaken. Sail shape is critical for two reasons. First, global shape affects torques (in-flight) that are caused by an offset between the center of pressure cp and the center of mass cm. In a gravity environment, the billowed shape (1/2-m-overall gravity-induced sag) is deep enough to affect the modal response of the sails. The ability to confidently predict approximate frequencies of the first few system modes is essential for control system design needed for flight. Second, fine-scale topology affects the overall thrust performance of the sailcraft. Personnel at LARC employed a laser radar-scanner system to provide measurement of the entire sail surface with an accuracy better than 1 mm. Shape data were obtained for both the RS5 and RS3 sails, and comparisons on the measured and predicted global billow shapes were in reasonable agreement, typically within 3 cm across the 10-m sail. A second ambient deployment was conducted on 6 April when, again, data on mast and sail deployment speed, motor current (convertible to lanyard and halyard loads), and tack-line tension were recorded, as well as images from two fixed-position digital cameras and three pan-zoom video cameras. An image from one of the digital cameras is shown in Fig. 2. The repaired tear is evident at the right. The gossamer masts are hardly visible in the figure, but the

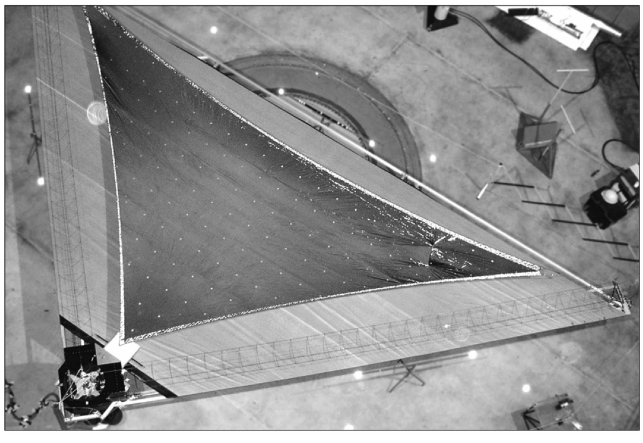

Fig. 2 10-m quadrant test at 16-m LARC vacuum facility.

distribution of photogrammetry targets and the compliant sail borders are brightly lit.

Mast dynamic testing was performed with excitation input at the sixth bay. Using laser vibrometer targets at the mast tip, the first in-plane and out-of-plane bending vibration modes and the first torsional vibration mode were captured. Greater mass distributed along the mast (harnessing and vibrometry targets) and at the tip, in combination with the central structure and GSE flexibility, resulted in lower mast frequencies (4.4 vs 5.7 Hz) than were recorded during earlier component-level testing at ABLE and that were slightly lower than predicted (4.7 Hz) for the integrated masts. The first four modes of the system were captured in test, and overall the agreement between the predicted and measured shapes was reasonable. The first-mode frequency prediction by finite element analysis was lower than that found in the test. This discrepancy could be expected given that the finite element analysis overpredicted the billow depth (likely due to halyard tension uncertainty and load angle variation), which can account for an underprediction of the first-mode frequency. The higher-frequency mode shapes measured were as predicted. The frequency predictions were generally higher because they are more dependent on mesh density, the effective extensional modulus, and the stress distribution, which are interrelated in the prediction of local shape and stiffness.

V. Scalable Full-System Demonstration

A. Design Evolution

The soundness of the fundamental elements of a deployable integrated sail and structure were validated with the tests performed on the 10-m quadrant. But the low fidelity of the central structure and the lack of representation of a full compliment of sails and other hardware needed to complete the S^4 architecture left a significant level of uncertainty in the 20-m system design definition. In addition, the system definition began shortly after analytical correlation and reporting on the quadrant test series. Major elements added to the design consisted mainly of attitude-control mechanisms. But the chosen implementation forced complete redesigns of the tip and central structure mechanisms, as well as the incorporation of associated actuators and electronics. Demonstration of a flight-fidelity central structure and the pursuit of an integrated sailcraft philosophy (rather than a propulsion "backpack") were also major objectives that were achieved. The major changes and challenges between the 10 and 20-m systems are summarized in Table 1.

Another element incorporated into the 20-m system was a payload instrument boom. In the original S^4 sailcraft concept [2], a similar appendage was used to extend the spacecraft host bus away from the sail so that it could be gimbaled to provide propellantless attitude control (pitch and yaw). In phase 2, after a detailed trade study of ACS options was undertaken [15], an alternate approach was adopted. However, an instrument boom demonstration was retained due to its general utility for offsetting science payload away from the plane of the sail. The baseline S^4 design offers the option for an instrument boom(s) to deploy instruments fore and/or aft of the sail. The maximum length of instrument boom (that stows fully within the central structure, which is not a requirement, but was demonstrated) is approximately 25% of the square sail size. The 20-m system was configured for instrument deployment 2.3 m to the antisun side, because this direction is preferred for an earth-orbiting validation mission. The mass of the bus components on the sun-side deck of the central structure could be balanced by the instrument mass (e.g., cameras), given the proper boom length, to create an attitude-neutral sailcraft. This is preferred to a cp-behind-the-cg stability approach for the reasons given in [15].

In a solar sailing demonstration mission of the S^4 technology, the need for photogrammetry is weak to nonexistent because the sails will be nearly flat (1-cm depth at 1 psi and 5 cm at 0.1 psi), unless a deployment anomaly occurs. However, cameras are invaluable for documenting the deployment, particularly the membrane management, and would also be invaluable for investigating anomalies if they occur.

B. Description of the 20-Meter System

The evolved S^4 sailcraft system integrates the gossamer coilable mast and sail membrane technology, solar arrays, launch tie-down and release mechanisms, and attitude-control actuators. Each of these items are efficiently packaged within structure shared by other bus components and mission payloads. These subsystems together form a generic scalable sailcraft possessing reliable deployment, structural robustness, and determinate sail shape with, *most critically*, minimized overall mass and volume. Computer-aided design (CAD) representations of the 20-m S^4 sailcraft system built in phase 3 are shown in Fig. 3. The mast structures used on the 20-m system were "truncated" in length, meaning that the diameter (40 cm) was sized for the needs of an 80-m system. Because the system "size" is 20 m from mast tip to mast tip, approximately 14-m-long masts were required. The central assembly, approximately 1 m across, was sized to hold enough mast structure for a 40-m sail system. The sizing choices for the central assembly and masts were made to allow the maximum benefit from design, fabrication, and validation activities in the ground demonstration toward a flight validation of a 40-m-class S^4 sailcraft.

The packaged sails and masts are arranged symmetrically around a central bay that houses the stowed instrument boom and mechanisms used for tie-down release of coilables and sail-bay panels (solar arrays), deployment of the coilables, and ACS mechanism control. The remaining volume is used to store the sails, which are packaged on drums with rate-limiting constant torque dampers and load sensors. Only a single motor is needed for deployment of each structural axis and, later, to control ballast bar position for attitude control. During deployment, the tie-downs and instrument boom are released first. Next come the sail mast pairs, deployed sequentially under rate-limiting control of a common lanyard-tape spool (part of the central mechanisms). The coilable self-deploys by using the strain energy stored in the stowed longerons. To assure kinematic determinacy, the base end is biased to uncoil first, and the transition zone progresses outward with the tip as the lanyard is reeled out off a

Table 1 20-m vs 10-m system changes and challenges

S^4 system	Quadrant took advantage of the quarter-symmetry of a square sail. The 20 m is a complete system, structured to act as a sailcraft bus chassis, with integral solar panels, ACS, and payload adaptor fitting interface.
Mast assy	Added elements added inside each batten to guide the traveling ballast bars (ACS pitch and yaw control) down the centerline.
Sail assy	Four times larger. Thinner material, shallower scallops, thinner cords, and ripstop elements. Folded first in a direction opposite to the 10-m sail design. Deploy sequencers moved to edge cords and redesigned.
Central structure	The 10-m central assy was a low-fidelity aluminum structure that served as a volumetric housing for the masts and sail (and the first-generation deployment mechanisms). The structural approach was upgraded to a flightworthy lightweight construction.
Central mechanism	With the addition of ACS elements, a complete redesign of the central mechanisms was needed to provide shared functionality between the ballast bar control and mast and instrument boom deploy functions.
Mast-tip mechanisms	For the addition of movable spreader bars for roll ACS, mechanism needs at the mast tips increased significantly.
Electrical sensors and drivers	Added to central assy and tip plates: motors/driver boards for reeling up the sails at the mast tips and for running the ballast masses, limit switches and optical sensors to provide end-of-travel indications, load cells for added sail deploy diagnostics, and μPPT controls.

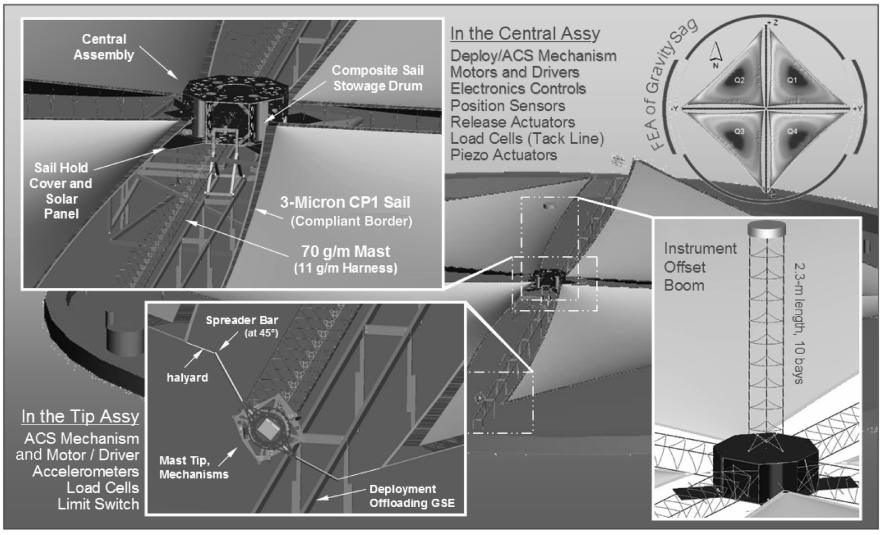

Fig. 3 Depiction of a 20-m S^4 system in the Plum Brook chamber, with details of critical elements.

pulley by a rate-controlled stepper motor. With the masts fully deployed, the sails are deployed next, in unison, by motors at the mast tips. Later, the same motors are used for spreader-bar rotation (roll ACS). Sequential deployment staging simplifies mechanization, increases ground-testing fidelity, and improves reliability.

As shown in Fig. 3, the sails are connected to the structure at three points, which provides for a deterministic structural loading condition and assures a planar sail shape. At the tips of the masts, adjacent sails are tied to a spreader bar with near-constant-force (negator) springs to assure steady tension regardless of sail temperature, which varies with solar orientation. If all of the spreader bars are rotated out of the nominal sailcraft plane in unison, the sail quadrants form a slight "windmill" shape. Solar forces then create a moment that can used for roll attitude control. Pitch and yaw control are integrated into the sail system by using the mechanisms in a dual-purpose manner; that is, each mast axis is deployed with a motor-controlled lanyard, then this motor and lanyard are used to move a ballast bar that adjusts the *cm* relative to the *cp* of the sail.

The 20-m S^4 system demonstrated a significant number of embedded control systems and sensors. The utility of each in a flight application can be most easily summarized by following the chronological order in which they are employed, following the initiation of deployment. First, the firing of the separation nuts indicates the tip-plate release (one per mast). Their current is monitored to insure that heating of the actuating element is occurring. This activity can be validated with colocated thermal sensors. The initial motion of each mast when the tie-down is released can be validated by the accelerometers on each mast tip. Each sail-bay door (which also functions as a solar panel) opens when the adjacent mast "kicks over" (rapidly straightens) at the base (when about eight bays are deployed). The dynamics reactions of the masts kicking over and the panels releasing will also be evident in the accelerometer traces. The advancing step count of the mast deployment motors (one per axis) provides an indication that the mast pairs are deploying nominally, driven by their stored internal strain energy (they are retarded by the motor/lanyard system).

Once the final kick-over of each deployed mast has been indicated by the accelerometers, piezoelectric actuators located in line with the mast longerons at the root can be used in conjunction with the accelerometers to measure the bending modes of the masts (before sail deployment). The sails are hoisted using halyards that are reeled up onto spools at the mast tips. Halyard tension is monitored by load cells throughout deployment, providing feedback to indicate completion. The load is also monitored during flight of the deployed system, to indicate changes in load with spreader-bar angle adjustments. The sail drum is mounted with a load sensor at one end of the rotational axle. This arrangement allows the load into the sail at the "tack" corner to be monitored while the sail is deploying, and it also provides the load in the deployed sail during the mission. The three-point suspension configuration, with load sensors at each point, provides redundancy in the deployed system state knowledge. The load profile during deployment has peaks that occur as each sequencer loads up and then releases. Between sequencer events, the load is a function of the retarding torque provided by the damper on the drum. The accelerometers on the mast tips also provide a backup record of the timing of the sequencer releases as the sails deploy. They also allow assessment of the dynamic modes of the fully deployed system and information about how the structure reacts to attitude-control maneuvers. The same accelerometers, which resolve steady-state loads, can monitor sailcraft spin rate if centrifugal forces are used to assist deployment. However, these data will likely be secondary to higher-fidelity telemetry obtained from spacecraft attitude determination and control subsystems (ADCS).

Spreader- and ballast-bar positions are controlled and monitored based on motor step count, and home switches are included to allow position reset in case the absolute step count is lost. The electronics and stepper motors located on the mast tips are kept warm by a thermostatic heater circuit. And temperature is monitored at the tie-down actuators, at the central motors, and at other key locations by numerous resistance temperature detectors (RTDs).

All of these embedded elements were present and validated on the 20-m sailcraft system at Plum Brook. The information that can be captured by clever employment of these devices will form an invaluable supplement to the critical deployment video (low-capture-rate, sequential, still images) acquired by cameras offset from the plane of the sails by the instrument boom. A ground-controllable pan-tilt camera would be ideal for tracking particular areas of interest such as boom uncoiling, lanyard advancement, tip kick-over, ballast movement, spreader-bar motion, halyard mechanization, sail synchronization, and inspection of deployed-sail surface morphology. Documentation of the deployment process is of primary interest, followed by identification of the sail shape and the fundamental system modes. Because the sail is nominally flat and the targets will have been applied at known locations, the verification of a nominal global, billowed shape can be accomplished with photogrammetric analysis of images from a single camera location. Local shape inspection will be aided by changing lighting conditions. The fundamental system mode shapes may be captured with videogrammetry, but would require high camera resolution and large targets. Because of the small displacements involved, a more practical instrumentation option is an accelerometer. The 20-m system demonstrated the inclusion and operation of a suite of accelerometers, a host of other embedded systems, and a camera platform, for full characterization and in-flight behavioral identification.

Attitude control after tip-off, during deployment, while sailing, and after sail jettison must all be accomplished with reliable and low-mass solutions. The S^4 sailcraft system uses a propellantless

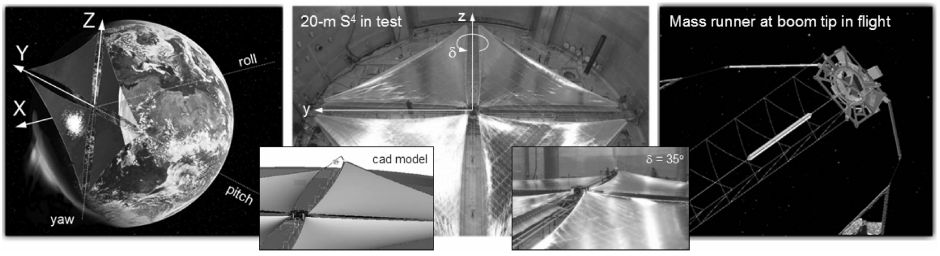

Fig. 4 ACS coordinate definition and depictions of systems in use.

method of three-axis control (described previously herein) that relies on solar pressure acting on the extended sails. For a mission in which the sail is jettisoned at some point, a traditional bus ACS may be employed, and it may also be used during deployment. Thrusters may be a more cost-effective method for control of a validation mission, given its brief mission needs. The propellant tank can be sized to also perform a deorbit maneuver if needed. Recommendations for primary, secondary, and backup ACS types and control during deployment and other mission scenarios are discussed in detail in [15]. The primary sail-based ACS together with a reaction gas system on a host spacecraft is a robust pairing for flight validation and follow-on missions [16]. For typical science missions, backup control of a large sailcraft could potentially expend all gas reserves and would require impractically large wheels. A secondary ACS using mast-tip-mounted pulsed plasma thrusters (PPT), *a lighter-weight, lower-cost, robust alternative to traditional methods*, was detailed in [17,18]. PPT-based ACS provides more reliable capability for recovery of attitude given any off-nominal conditions, including tumbling, that cannot be handled by either the propellantless primary ACS or by the conventional ACS within, at the center of the system. PPT attitude control would be particularly useful for three-axis stabilization of a sailcraft after release from the launch vehicle, during deployment, and for preflight sail checkout operations on a science mission in which total mass is at a premium, secondary control is warranted, and the sail is not jettisoned before the completion of the mission. Discussion of the state of the art in miniaturized, often denoted "micro," PPT (μPPT) technology, performance requirements for solar sails, and pulse-modulated control design and simulation results were presented in [17]. Development and test of a demonstration system is reviewed in [19].

The 20-m sailcraft hardware demonstrated the rate and range performance of the mechanisms used to provide primary roll, pitch, and yaw. It also demonstrated the interfaces necessary for μPPT thrusters, with associated wiring and control, at the tips of the masts. The coordinate definition, the 20-m system with spreader bars (roll control) positioned from 0 to 45 deg, and, approaching the mast tip, a ballast bar used for pitch and yaw control are shown in Fig. 4. This lightweight, robust, propellantless ACS can be appropriately sized and designed to meet the requirements of a wide range of missions [15]. For example, a 40-m-class sailcraft has performance and stability characteristics allowing a 35-deg attitude maneuver within 2 h, a thrust vector pointing range of 60 deg, a thrust-vector-control (TVC) pointing error of less than 1 deg, and a TVC pointing stability (jitter) of less than 0.01 deg.

The standard robust proportional–integral derivative (PID) control logic (with saturation control loop) investigated by ASU provides zero steady-state pointing errors of the bus-fixed reference frame, even in the presence of constant solar disturbance torques. However, in practice, there are always unavoidable (but small and acceptable) control-loop hardware errors caused by attitude sensors and actuators (misalignments, resolution, noise, etc.) that may require inclusion in the ACS model. Thrust-vector-control pointing can be based on a simple solar radiation pressure (SRP) model, but errors associated with imperfections (reflectivity, billow, creases, etc.) should be included to more closely predict the actual magnitude and direction of the thrust vector. Parametric tools for the evaluation of influences such as billow shape on sailcraft thrust are of great utility [20]. A comprehensive evaluation of the influences of various types of imperfections on sailcraft thrust has been recently completed by ATK as an input to the Solar Sail Control Toolbox (SSCT) under development by PSS [21]. In the effort to model propulsive thrust, finite element modeling was first used to determine the shape of a sailcraft under combined solar pressure and inertial loads. A parametric tool was developed to allow the evaluation of specular reflection, diffuse reflection, and thermal-emission thrust components as a function of the sailcraft-to-sun angles, local topology, sail thickness, temperature, and stress. Variations in optical properties, fabrication tolerances, and sail damage effects on the vehicle thrust and moments can be evaluated and graphically trended with this tool. An example of the findings (see Fig. 5) illustrate the importance of accurately modeling sail shape. Figure 5 shows the offset in the cp location from the sailcraft center increases as the sailcraft is canted. Lower sail-tension system designs result in lower system mass, until the attitude-control subsystem mass, *properly sized to counteract the offset torques*, becomes dominant. Application of this type of modeling rigor insures that proper design margins for authority over solar pressure asymmetry (and required maneuvering) torques are included in the development of the vehicle control system. A low-sail-stress design will have a very low first system-vibration frequency, which may also complicate the design of a stable control system. Although control modeling with flexible-body dynamics has only been initially investigated at this time [22], it is within the capabilities of the system modeling tools developed by PSS. With structural inputs from the sailcraft designer, ACS margin evaluation from a parametric propulsion vector analysis, and a mission definition from NASA, the SSCT can be used to accurately characterize sailcraft performance for a multitude of parameters in a trajectory propagation analysis.

C. Overview of the 20-Meter Sail Testing Activities

During the assembly of the 20-m system, component evaluation was completed by informal engineering evaluation of form, fit, and function, with some subassembly testing undertaken for risk reduction. The accelerated schedule included significant design modifications to testbed hardware, made in parallel with system assembly. The completed assembly passed general electrical and physical inspections, but there was only time for a few partial-system (one or two of four sails installed) deployment trials before it was necessary to prepare the 20-m system for shipment to Ohio for testing in the 100-ft vacuum chamber at the NASA John H. Glenn Research

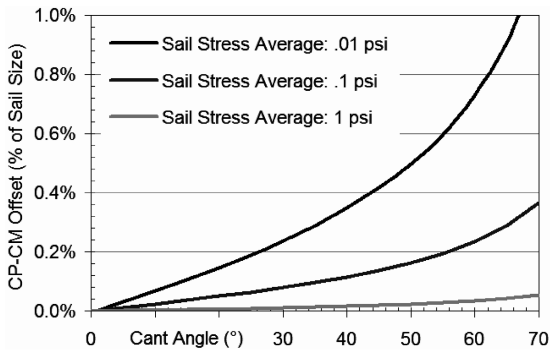

Fig. 5 Center-of-gravity offset induced in imperfect sails vs cant orientation.

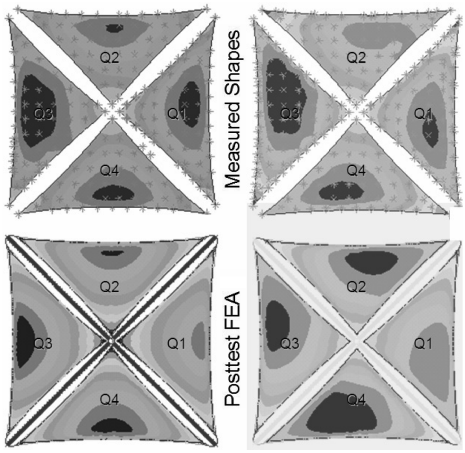

Fig. 6 Sail shape predictions vs test results.

Center's Plum Brook station [23]. The primary formal tests for S^4 demonstration and validation were performed at Plum Brook. The priorities for this activity were to demonstrate the deployment robustness and to capture sufficient shape and dynamics data to permit validation of FEA models. The ATK–LARC test team executed an extensive series of tests [24] to capture the data needed to support these priorities, as well as to meet goals for developing test methods applicable to larger-scale testing and to in-flight investigation.

Three full-system validation deployments were completed: the first in ambient, the second in vacuum, and the third (also at 10^{-5} torr) with a thermal gradient imposed across the stowed system. During the third deployment, an intervention was required to correct a simple integration error that led to halyard corner entanglement. Otherwise, the three deployments were successful. The key analytical validations for the 20-m system paralleled activities performed on the 10-m quadrant in phase 2, namely, shape and dynamic characterization. To capture shape data on the effects of gravity on mast droop and sail sag, LARC personnel employed five photogrammetry cameras to measure the system at three spreader-bar positions (nominal and the two extremes). To capture dynamics data, LARC personnel used both external inputs and response sensors to measure the first modes and modal frequencies of the system and embedded actuators and sensors that are applicable to a flight program. Shape and dynamics data compared well with pretest analyses [25]. A review of the testing and model correlation and validation findings for each is given next.

D. Shape Testing and Model Validation

Measurements of sag induced by gravity are predominately related to the sail quadrants. The central structure was supported by a support frame. Each deployed sail was supported only at three corners, to the S^4 structure at the nearest two mast tips and at the central structure, to its stowage drum. Negator springs at each mast tip were balanced to support the tip at the same level as the mast root, with the sails deployed. Each of the sails was delivered by SRS outfitted with a series of 41 1-in. retroreflective targets in the field, plus three at the sail corners. Photogrammetry targets were placed on the mast tips to capture in-plane mast-tip motion (due to quadrant mass differences) and on the spreader-bar ends to allow the bar rotation to be tracked as they were actuated +45 deg. The tip positions and sail sag and reference targets were then measured by photogrammetry cameras under low- and high-intensity lighting. Shape testing with the spreader bars at 0, 22.5, and 45 deg was completed. Typical measurement precision out-of-plane was 0.5 mm.

The billow shape imparted to the 20-m sail in 1 *g* is analogous to the billow induced by solar pressure in space, but 200 times greater. The stress in the sail is also significantly influenced by gravity. The nominal stress is nearly 20 times higher, and uniform stress conditions are no longer achievable. About half the load that would normally be carried uniformly across the compliant borders and into the scallop cords is instead carried by jumper straps at the sail corners. Consequently, the load sensors in line with the halyards and tack line do not represent the cord loads alone but also the load shared by the jumper strap. This gravity-induced condition complicates the prediction of sail sag greatly, compared with zero-*g* modeling, in which the load path is more deterministic.

The test findings for the system are graphically compared with the FEA modeling in Fig. 6 and Table 2. Results are shown for 0 and 22.5-deg spreader-bar angles, on the right and left, respectively. The error in the FEA prediction for the maximum sag deflection point of Q4, the most flightlike sail, was 10%. In general, the FEA correlation did not improve when the model was updated to include measured test conditions for halyard loading and to capture the fact that the jumper strap on the inboard corner of Q4 was broken. The halyard load assumption was 6 lb each for pretest analysis. The loads were actually 4.1 to 6.7 lb in the test, but due to the difficulties in obtaining (1-*g*) sail-model convergence, the loads were updated to the *average* for each sail's halyard load. This modeling expediency was judged reasonable, because the loads themselves had a +20% uncertainty due to friction in the halyard negator mechanism. The accuracy of the FEA prediction was improved relative to the 10-m results, even though the modeling was complicated by the sail being twice as large, the jumper straps carrying load, and the mass differences between the cosuspended sails. The latter effect caused the mast tips to move in-plane, leading to asymmetry in the halyard angles. Additional testing was performed with the goal of measuring the shape of a sail without the influences of other sails or halyard hysteresis. Testing was performed at SRS under three specified load conditions on quadrant 4. Photogrammetry was used to identify the membrane surface target locations in three dimensions and the location of the support-line terminations. Simple low-friction pulleys and dead weight were used to load the outboard sail corners precisely to 6 lb. These simply guaranteed boundary conditions (line angles and loads); the same sail model correlated to the measured shape with an accuracy of less than 1%.

E. Dynamics Testing and Model Validation

The 20-m S^4 system is shown in Fig. 7, as oriented inside the Plum Brook vacuum chamber in the deployed test configuration. The coordinate reference frame, quadrant numbering, and excitation locations are indicated. Retroreflective targets on the sails, mast tips, spreader bars, and various scale bars (used for photogrammetry) are also visible. Baseline sail dynamics testing at Plum Brook took place at pressures from 1–2 torr.

Measurements of dynamic response were made primarily at the 44 retroreflective targets on the sails, using a laser vibrometer. Baseline testing used dynamic excitation by magnetic forces (noncontact) at the quadrant corners. Other excitation methods were evaluated for their suitability to on-orbit modal investigations, such as piezoelectric stack actuation from the mast roots, spreader-bar rotation (at the mast tips), and bimorph piezoelectric patch actuation on the sail cords. The masts were tested separately, using piezostack

Table 2 Maximum billow prediction correlation

Q	As tested at 0-deg spreader	FEA pretest	FEA post	Q	As tested at 22.5-deg spreader	FEA pretest	FEA post
1	54 cm	−6%	5%	1	48 cm	−2%	6%
2	52 cm	9%	16%	2	45 cm	15%	20%
3	59 cm	−6%	12%	3	54 cm	−5%	5%
4	54 cm	9%	16%	4	50 cm	10%	18%

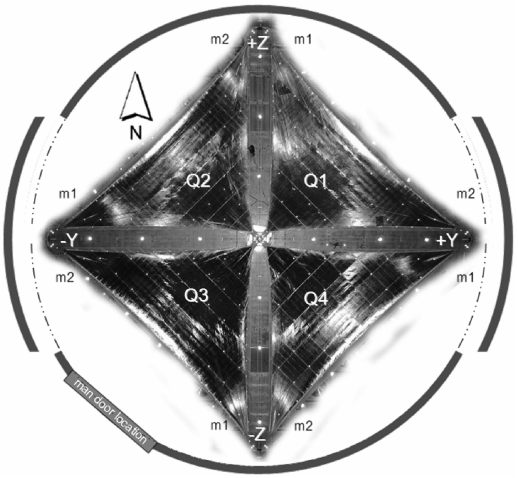

Fig. 7 The 20-m S^4 system in the 30-m vacuum chamber at Plum Brook.

actuators (in ambient atmospheric conditions) to provide a baseline for the response of these primary structural members. This approach could be followed in-flight as well, given sufficient time is arranged before the deployment of the sails.

The first two modes were found to agree within 1% on all four masts. The frequency responses for the *Z*-axis mast are shown in Fig. 8a, on the left. The first mode, at 0.81 Hz, represents cantilever bending in which the tip moves in-plane, with slight pendulum-effect-stiffening from the 1.8-m overhead support cable. The second mode is driven by mast torsional compliance and the tip-mass rotational inertia. The third peak is attributed to the tip mass bouncing vertically on the support cable. The fourth peak corresponds to the second in-plane bending mode. The response of all four masts during *system* testing is shown in Fig. 8b. The modes are lower because the masts are supporting the weight of the sails. For system testing, the changes in tip offloading consist of the addition of a negator spring in line with the support cable (at the top) and a 2.3-kg counterweight mass added to the tip plate. The negator spring system provides a low-frequency suspension to free up system modes that are out-of-plane. The counterweight mass is cantilevered one-half meter above the tip plate, to counteract the torsion imparted by the sail halyards when the spreader bar is rotated away from the 0-deg (balanced) position. Increases to the effective rotational inertia at the tip cause the first twist mode to drop to 0.50 Hz. The second clearly visible peak is a combined twisting and bending response at 1.06 Hz. The in-plane mode was not captured because the reflector aligned to register mast lateral motion was not captured in system testing. The observed modes agree to within 2% relative to the pretest predictions. Excitation responses of the masts with the piezostack actuators produced clean response peaks (note that the data in Fig. 8 are plotted in a semilog format). This mode of excitation, originally developed for the SAILMAST flight experiment [11], will be validated in space in 2009.

Measurements of system dynamics were made for various magnet-excitation combinations and input parameters, at both the quadrant level and system level. Bending and torsion of the masts dominate the lowest modes of interest on the 20-m system. This response is due mostly to the presence of the eccentric counterweights mounted to the mast-tip plates. The counterweight reacts the torque induced on a mast that develops from the tensions of the opposing sail halyards as a spreader bar is tilted. This mass had to be used when the spreader bar is at 0 deg as well, because the offloading negator provides tip support to only the nominal weight.

For the baseline test configuration, the sail spreader bars were horizontal and then they were rotated 22.5 deg for another sequence of tests. Similar modal responses were seen in the four sails at each position. The range of expected modes and test findings for the baseline sail (Q4 was the most representative of the intended flight design) at the nominal spreader-bar orientation (0 deg) are shown in Fig. 9. Listed in the gray bar regions aligned along the graph of target responses are the dominant expected mode frequency ranges. The responses that fell below the response of the target beside the excitation input (bold line) were trimmed out for clarity. The first grouping of peaks indicates fundamental modes in the range of 0.50 and 0.62 Hz. Each of the sails has a slightly different mass and so this creates sets of four spread low-frequency responses, one for each sail's fundamental mode. As shown in the inset to the graph in Fig. 9, the lowest mode responses for M2-excitation were similar to that of the M1-excitation results.

The shape predicted by FEA corresponding to a fundamental mode of Q4 at a frequency of 0.483 Hz is shown to the right of the graph in Fig. 9, above the operational deflection shape (ODS) found in the testing. The same response (0.50 Hz) was found for various inputs [i.e., at magnet 1 (M1) and at magnet 2 (M2)] and for out-of-phase excitation of M1 and M2. The second mode, shown to the right in the figure, corresponds to mast bending. Again, there were four related modes predicted (from 0.62–0.64 Hz) for various combinations of mast motion phasing. The modal responses found in the test peaked at 0.625 Hz for the three input conditions, but the ODS shape recorded for each varied slightly. As can be seen in the three quadrant details in Fig. 9, the nodal line shifted toward the input, as may be expected in a very flexible nonlinear system.

The best location for modal excitation is, ideally, at the antinodes of the system response. Magnets were positioned at the three corners of the sail and at the middle of the hypotenuse cord. The latter was unusable due to variations in the sail position after pump-down. Condensation formed on the membrane as the chamber was initially evacuated. This increased the effective mass of the sail and the negator-spring-mounted halyards were extended. When the chamber reached a substantial vacuum, the water evaporated, returning the supported load to a nominal value. A small amount of positional variation (due to hysteresis) in the negator mechanism was amplified to result in a positional variation of 5 to 15 cm at the midpoint of the

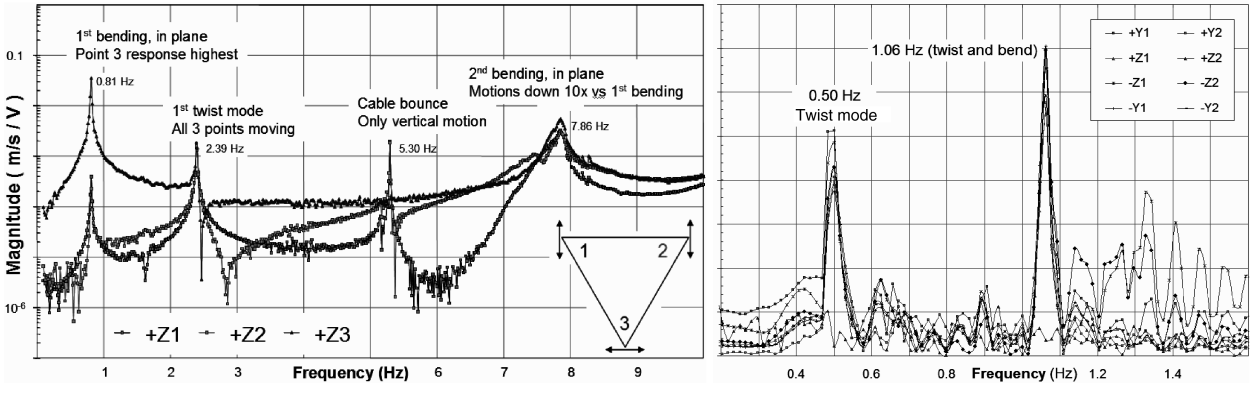

a) b)

Fig. 8 Mast tip responses a) in ambient conditions and b) with sails and counterweights in vacuum.

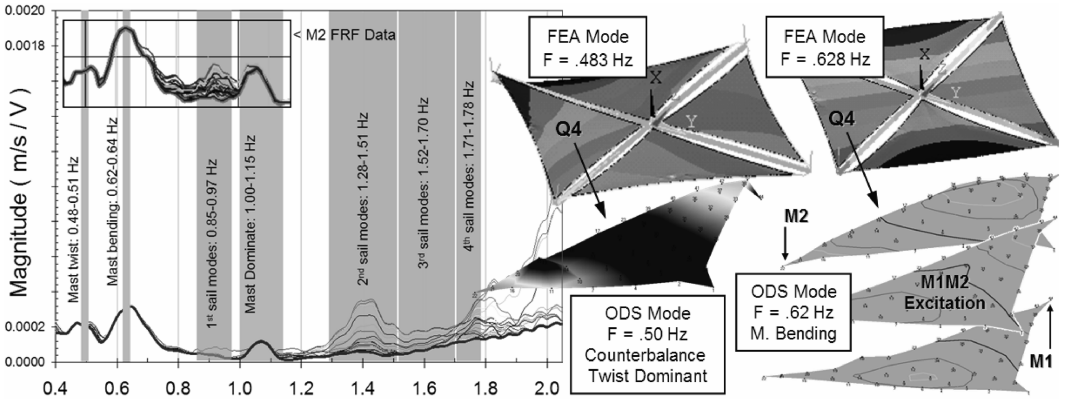

Fig. 9 System dynamic responses to M1 input, lowest modes due to mast-tip counterweight.

sail hypotenuse. This variation was greater than the stroke of the magnet-position adjustment actuators, and the testing schedule did not allow time for diagnosis, mitigation testing, and added pump-down days.

F. Launch Survivability Validation

After the final stowage of the S^4 system at Plum Brook, the assembly was returned to ATK-Goleta to be outfitted with mass simulators in preparation for vibration testing. Four masses, totaling 50 lb, were distributed across the top deck, representing bus and payload components commensurate with an optimum sailcraft mission configuration. An additional 4-lb payload mass was mounted to the tip plate of the instrument boom. The assembly response to a low-level sine-wave input and the survivability under a launch random vibration exposure were investigated. The lowest modes of the system were evident in the response to both inputs. The first mode of the system was near 81 Hz, comparing closely with FEA prediction of 83 Hz. The random environment levels, 14 $g_{\rm rms}$ from 20–2000 Hz for 60 s in three axes sequentially, was constructed to envelope the likely launch vehicles for a payload of this size, including Minotaur I/II and IV, Taurus, Pegasus, and Falcon. After vibration testing, inspections and a partial deployment test were conducted to validate the survival of the at-risk structural and mechanical aspects of the system. The only evidence of damage was found on the *Y*-axis mast: A batten rod debonded at bay 7 and a diagonal in bay 1 was broken. It was recognized in development testing that the batten fitting bond length was insufficient. Small secondary straps had been applied to strengthen the bonds at the 1488 rod ends, rather than remaking the batten assembly due to schedule pressure, and so a debond was not surprising. The diagonal failed at the mast terminal end fitting. The design employed (based on existing heritage) was larger than the optimized cup fitting used on the other 99.2% of the mast. To allow the small cabling to seat in this cup, a larger ball was swaged on the inboard end. This swage overstressed the cable and led to breakage after repeated cycling. Given the minor and correctable issues uncovered, it can be extrapolated that a future S^4 sailcraft would have a high probability of surviving the launch vibration environment.

A second environment against which the S^4 technology was evaluated is the rapid depressurization that occurs during launch ascent. Because only the sail is vulnerable, a packaged sail/drum assembly was tested in a representative sail-bay enclosure. The depressurization profile of a Delta II launch was applied in a vacuum chamber that allowed viewing of the article. No material billowing was evident: the fold and roll packaging left short path lengths for air evacuation. A posttest deployment of the sail was nominal, with a single exception: during deployment, one of the sequencer straps was found to have been improperly prepared, *lacking a key feature to provide low controlled breaking strength*, and had to be manually separated as the sail deployed. This deployment marked only the second time (in 13 formal sail deployments) that a quality-control issue had prevented full success. The repetitions of deployments (including the 17 informal 20-m sail deployments) in the SGD program provided invaluable insights into the methods and checks needed to ensure deployment success.

VI. Sail Membrane Life Testing

Samples of sail material (2.5- and 5-μm aluminized CP1) were exposed to various space environmental effects. Testing at the MSFC SEE laboratory included electron, proton, UV, and micrometeoroid exposure. Optical (reflection, transmission, and specularity) and mechanical (modulus, stress and strain to failure, and cyclic stress fatigue limit) properties were measured before and after exposure. The solar-averaged reflectivity of the aluminized sail material was baselined at 91.8% (+0.3% over 30 samples). Transmission through the 800-Å aluminum coating was undetectable. Exposure to 250–400 nm near-ultraviolet (NUV) radiation was at an intensity of two suns. Increased curling of the samples was observed during the first 250 h of exposure, but optical properties were unaffected by the 1000-h (80-day equivalent) test.

The radiation fluence for the three-year Solar Polar Imager (SPI) mission was estimated, and the material was exposed to various flat-dose levels with 50- and 700-keV protons. As shown in Fig. 10, a 5-Grad flat-dose electron exposure is well in excess of the average dose at depth for the SPI mission. A 5-Grad flat-dose proton exposure is

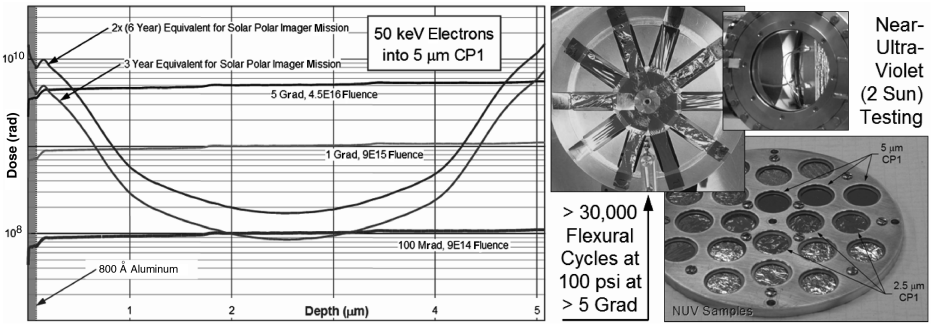

Fig. 10 Sail-material life testing: flat-dose *e* and *p* radiation, flexural cycling, and UV exposure.

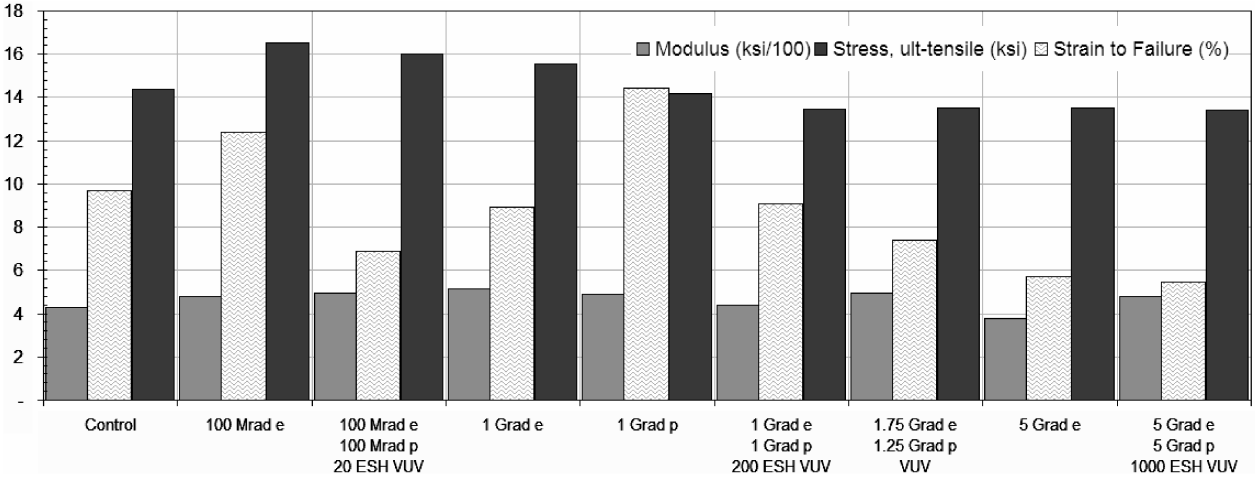

Fig. 11 CP1 properties variation as a function of dose (ESH: equivalent sun hours, VUV: vacuum ultraviolet).

more than two times the expected dose at *every* depth. The L1 mission environment is much less severe, per year, than the SPI mission (at 0.48 AU).

Five or more 5-μm samples were subjected to various exposures (bounded by a combined 5-Grad electron, 5-Grad proton, 1000-VUV sun hours case), then removed from the chamber and tensile tested. There was little change in modulus or strength (nominally, 430 and 14.4 ksi, respectively), and the material maintained more than 50% of the control sample ductility (strain to failure). The property variations for all exposures are shown in Fig. 11.

Samples of 2.5 and 5-μm CP1 were also tested under cyclic loading conditions (0–100 psi) while being exposed to 50-keV electrons. Three 5-μm CP1 samples survived 14 Grad and 70,000 cycles and demonstrated an average ultimate stress of 7.2 ksi at the conclusion of testing. Two 2.5-μm CP1 samples failed during testing, one at 7 Grad and 30,000 cycles, and the other at 12 Grad and 50,000 cycles. When tested without cycling, the 5-sample average failure stress after 14 Grad electron fluence exposure was 10.5 ksi for 5-μm samples and 7.8 ksi for 2.5-μm samples. These tests demonstrate the robustness of CP1 as a sail material, in light of the fact that the nominal operation stress of a sail is 1 psi.

The CP1 material performed well in all aspects of the simulated space-environment testing, demonstrating that the sail membrane can withstand space environmental influences beyond the level identified for near-term sailing missions. More detailed reporting of the testing performed is presented in [26].

VII. Scaled Performance

The ISP program set requirements for the performance of the demonstrated system, scaled to obtain a $10,000\text{-m}^2$ reflective area. The performance of the S^4 sailcraft system for the key program metrics, areal density and stowed volume, are shown in Table 3, above several other metrics of fundamental importance. The evolution of the original design changed the total mass estimate very little, but for the final design, we baselined a stronger coilable, which resulted in a less compactly stowed, scaled design and a slightly higher first-mode frequency.

The coilable sizing is directly related to the sail stress assumed. Investigations into the propulsive performance of a postpackaged membrane (crinkled-surface topology) indicated that the nominal sail stress (1 psi) can be reduced toward 0.1 psi. A number of other optimizations are planned for future systems, which could be implemented in a spiral development approach, such as thinner membranes, jettison of launch and deployment hardware, strategies for reduced complexity in attitude control, and stayed masts. None of these options is required for near-term missions such as HelioStorm (at L1) and Solar Polar Imager, because the current extrapolated performance supports these missions with an adequate performance margin. But future efforts will undoubtedly incorporate at least some of these methods for improving the key performance metrics of solar sails, such as characteristic acceleration (a_c, mm/s^2) and areal mass density (ρ_a, g/m^2). The options listed, in combination, are projected to reduce the areal density of a 160-m sail subsystem to 3 g/m^2. Scaled performance for other metrics (shape and frequency) of sails up to 200 m are provided in Fig. 12.

Another important parameter for solar sail propulsion is the maximum solar loading permissible. Missions such as solar sails on a Solar Sentinel (e.g., 0.25 AU) require, and outer planet explorers are enhanced by (travel time is reduced), a close-solar-approach capability. The temperature of a 2-μm CP1 sail at L1 is 31°C (and as low as 9°C if off-sun 35 deg). This same sail can be used for the SPI mission, which will operate at 156°C at 0.48 AU. The maximum temperature capability of CP1 is 250°C. By using a carbon-loaded CP1 ($\varepsilon = 0.8$), a temperature of 220°C will be reached at 0.2 AU. Close-solar-approach capability would support Solar Sentinel missions, is of benefit to outer planet explorers, and significantly improves the mission timeline for an interstellar probe.

VIII. Conclusions

Technological futurists have dreamed of sailing on starlight for more than a century. These possibilities have been an inspiration to poets as well [27]:

> I cannot cause light; the most I can do is try to put myself in the path of its beam. It is possible, in deep space, to sail on solar wind.

Table 3 ISP program requirements and other metrics of interest (sail area 10,000 m^2 reflective)

Sail system parameters	Program requirements	Phase 1 design	Final point design
Areal density	<12 g/m^2	10.8 g/m^2	11.3 g/m^2
Stowed volume	<1.5 m^3	0.9 m^3	1.5 m^3
First system mode estimate		0.02 Hz	0.03 Hz
Volume description (goal: fit within a 2.5-m fairing)		1.5-m diam by 0.53 m	1.9-m diam by 0.54 m
Total scaled S^4 system mass		108 kg	113 kg
Characteristic acceleration, a_c (example given with 130-kg bus and payload)		0.76 mm/s^2 (0.34 mm/s^2)	0.73 mm/s^2 (0.34 mm/s^2)

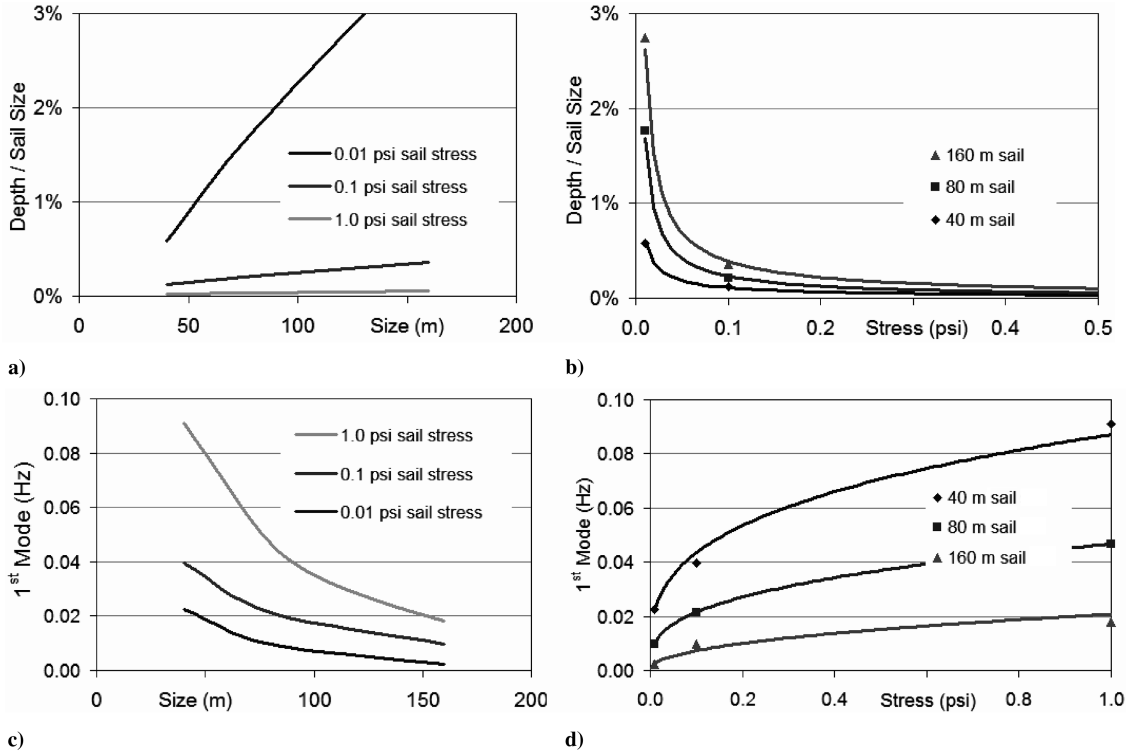

Fig. 12 Scaled performance: a) billow vs sail size, b) billow vs stress, c) frequency vs size, and d) frequency vs stress.

> Light, be it particle or wave, has force: you rig a giant sail and go. The secret of seeing is to sail on solar wind. Hone and spread your spirit till you yourself are a sail, whetted, translucent, broadside to the merest puff.

Imagination has become reality. The ground demonstrations and validations of S^4 system technology has elevated the technology readiness level (TRL) of solar sailing in all areas critical to support a flight validation mission in earth orbit. NASA's In-Space Propulsion Technology Program activities have systematically reduced the risk of flight implementation with substantial technology development through a series of demonstrations of increasingly more complex solar sail systems and by testing at the highest fidelity possible in the terrestrial environment. The progressive demonstrations of S^4 technology at the component, 10-m, and 20-m levels have elevated the TRL of solar sailing technology in all critical areas. The soundness of the design for deployment and control of a fully integrated sail and structure system has been validated through an extensive series of tests. Analytical correlation activities showed sound agreement with test results. The continuum of system design space and analytical modeling capabilities together ensure a functionally scalable design and mathematically predictable result for larger systems such as a flight demonstration system (40-m scale) and mission systems of up to 200 m on a side. It is time to set sail into space.

Acknowledgments

The work described in this paper was funded by the In-Space Propulsion (ISP) Technology Program, managed by NASA's Science Mission Directorate in Washington, D.C. and implemented by the ISP Technology Office at the NASA Marshall Space Flight Center (MSFC). This program would not have succeeded without the contributions of many individuals from the MSFC System Ground Demonstrator program, led by S. Montgomery, and at the NASA Langley Research Center, notably, J. Gaspar, T. Jones, and B. Taleghani, as well as B. Wie of Arizona State University and S. Thomas of Princeton Satellite Systems. Special thanks are given to P. Gierow, G. Laue, and J. Moore of SRS Technologies and to members of the ATK Space Systems and Sensors engineering team, P. Barker, R. Cope, M. Douglas, B. Macy, M. McEachen, A. Pavlick, P. Sorensen, R. Takeda, and T. Trautt, whose technical contributions and dedicated efforts made this paper possible.

References

[1] Garbe, G., Montgomery, E., Heaton, A., Van Sant, J., and Campbell, B., "NASA's Integrated Development of Solar Sail Propulsion," American Astronomical Society Paper 04-103, Feb. 2004.

[2] Murphy, D., Murphey, T., and Gierow, P., "Scalable Solar-Sail Subsystem Design Concept," *Journal of Spacecraft and Rockets*, Vol. 40, No. 4, July–Aug. 2003, pp. 539–547.

[3] Murphy, D., Trautt, T., McEachen, M., Messner, D., Laue, G., and Gierow, P., "Progress and Plans for System Demonstration of a Scalable Square Solar Sail," American Astronomical Society Paper 04-105, Feb. 2004.

[4] Gaspar, J., Mann, T., Behun, V., Wilkie, W., and Pappa, R., "Development of Modal Test Techniques for Validation of a Solar Sail Design," AIAA Paper 2004-1665, Apr. 2004.

[5] Murphy, D., Macy, B., and Gaspar, J., "Demonstration of a 10-m Solar Sail System," AIAA Paper 2004-1576, Apr. 2004.

[6] Taleghani, B., Lively, P., Gaspar, J., Murphy, D., and Trautt, T., "Dynamic & Static Shape Test/Analysis Correlation of a 10-m Solar Sail Quadrant," AIAA Paper 2005-2123, Apr. 2005.

[7] Murphy, D., Macy, B., and Gaspar, J., "Demonstration of a 20-m Solar Sail System," AIAA Paper 2005-2126, Apr. 2005.

[8] Montgomery, E., and Johnson, L., "The Development of Solar Sail Propulsion for NASA Science Missions to the Inner Solar System," AIAA Paper 2004-1506, Apr. 2004.

[9] Anon., "The Sun-Earth Connection Roadmap 2003-2028," NASA Goddard Space Flight Center, Rept. NP-2002-8-500-GSFC, Greenbelt, MD, 2002; also available at http://sec.gsfc.nasa.gov.

[10] Edwards, D., Hubbs, W., Stanaland, T., Hollerman, A., and Altstatt, R., "Characterization of Space Environmental Effects on Candidate Solar Sail Material," *Photonics for Space Environments VIII*, edited by E.W. Taylor, Vol. 4823, International Society for Optical Engineering, Bellingham, WA, 2002, pp. 67–74.

[11] McEachen, M., Trautt, T., and Murphy, D., "The SAILMAST Flight Validation Experiment," AIAA Paper 2005-1884, Apr. 2005.

[12] Crawford, R., and Benton, M., "Strength of Initially Wavy Lattice Columns," *AIAA Journal*, Vol. 18, No. 5, May 1980, pp. 581–584; also AIAA Paper 79-0753, 1979.

[13] Laue, G., Moore, J., and Clayton, W., "Innovative Structural Design Features for a 10-m Solar Sail Demonstrator," AIAA Paper 2004-1508, Apr. 2004.

[14] Laue, G., Case, D., and Moore, J., "Fabrication and Deployment Testing of 20-Meter Solar Sail Quadrants for a Scaleable Square Solar Sail Ground Test," AIAA Paper 2005-2125, Apr. 2005.
[15] Murphy, D., and Wie, B., "Robust Thrust Control Authority for a Scalable Sailcraft," American Astronomical Society, Paper 04-285, Feb. 2004.
[16] Wie, B., Murphy, D., Thomas, S., and Paluszek, M., "Robust Attitude Control Systems Design for Solar Sails, Part 1: Propellantless ACS," AIAA Paper 2004-5010, Aug. 2004.
[17] Wie, B., Murphy, D., Thomas, S., and Paluszek, M., "Robust Attitude Control Systems Design for Solar Sails, Part 2: MicroPPT-Based Secondary ACS," AIAA Paper 2004-5011, Aug. 2004.
[18] Wie, B., and Murphy, D., "MicroPPT-Based Secondary/Backup ACS for a 160-m, 450-kg Solar Sail Spacecraft," AIAA Paper 2005-3724, July 2005.
[19] Pryor, K., Wie, B., and Mikellides, P., "Development of a Lightweight Pulsed Plasma Thruster Module for Solar Sail Attitude Control," 18th Annual AIAA/USU Conference on Small Satellites, Logan, UT, Utah State Univ., Paper SSC04-XI-4, 2004.
[20] Moore, J., Gierow, P., and Troy, E., "High Fidelity Finite Element Based Modeling for Solar Sail Thrust Vector Prediction from Flexible Sail Models," *JANNAF Propulsion Meeting* [CD-ROM], JPM-CD-04, Johns Hopkins Univ., Laurel, MD, 2004.
[21] Thomas, S., Paluszek, M., Wie, B., and Murphy, D., "Design and Simulation of Sailcraft Attitude Control Systems Using the Solar Sail Control Toolbox," AIAA Paper 2004-4890, Aug. 2004.
[22] Thomas, S., Paluszek, M., Wie, B., and Murphy, D., "AOCS Performance and Stability Validation for a 160-m Solar Sail with Control-Structure Interactions," AIAA Paper 2005-3926, July 2005.
[23] Anon., "Space Power Facility (SPF)" [online article], http://facilities.grc.nasa.gov/spf/index.html [retrieved 20 Feb. 2007].
[24] Gaspar, J., Mann, T., Behun, V., Macy, B., and Murphy, D., "Testing of a 20-m Solar Sail System," *JANNAF Propulsion Meeting* [CD-ROM], JPM-CD-05, Johns Hopkins Univ., Laurel, MD, 2005.
[25] Taleghani, B., Lively, P., Banik, J., Murphy, D., and Trautt, T., "20-Meter Solar Sail Analysis and Correlation," *JANNAF Propulsion Meeting* [CD-ROM], JPM-CD-05, Johns Hopkins Univ., Laurel, MD, 2005.
[26] Edwards, D., Semmel, C., Hovater, M., Nehls, M., and Gray, P., "Solar Sail Material Performance Property Response to Space Environmental Effects," *Photonics for Space Environments 10*, Vol. 5554, International Society for Optical Engineering (SPIE), Bellingham, WA, 2004, pp. 80–91.
[27] Dillard, A., *Pilgrim at Tinker Creek*, HarperCollins, New York, 1998.

M. Nemeth
Associate Editor